1521-009X/49/5/379–388$35.00
Drug Metabolism and Disposition

https://doi.org/10.1124/dmd.120.000306
Drug Metab Dispos 49:379–388, May 2021

Metabolic Retroversion of Piperaquine (PQ) via Hepatic Cytochrome P450–Mediated *N*-Oxidation and Reduction: Not an Important Contributor to the Prolonged Elimination of PQ

Yuewu Xie, Yunrui Zhang, Huixiang Liu, and Jie Xing

School of Pharmaceutical Sciences, Shandong University, Jinan, China

Received November 4, 2020; accepted March 1, 2021

ABSTRACT

As a partner antimalarial with an extremely long elimination half-life (~30 days), piperaquine (PQ) is mainly metabolized into a pharmacologically active *N*-oxide metabolite [piperaquine *N*-oxide (PN1)] in humans. In the present work, the metabolic retroversion of PQ and PN1, potentially associated with decreased clearance of PQ, was studied. The results showed that interconversion existed for PQ and its metabolite PN1. The *N*-oxidation of PQ to PN1 was mainly mediated by CYP3A4, and PN1 can rapidly reduce back to PQ via cytochrome P450 (P450)/flavin-containing monooxygenase enzymes. In accordance with these findings, the P450 nonselective inhibitor (1-ABT) or CYP3A4 inhibitor (ketoconazole) inhibited the *N*-oxidation pathway in liver microsomes (>90%), and the reduction metabolism was inhibited by 1-ABT (>90%) or methimazole (~50%). Based on in vitro physiologic and enzyme kinetic studies, quantitative prediction of hepatic clearance (CL_H) of PQ was performed, which indicated its negligible decreased elimination in humans in the presence of futile cycling, with the unbound CL_H decreasing by 2.5% (0.069 l/h per kilogram); however, a minor decrease in unbound CL_H (by 12.8%) was found in mice (0.024 l/h per kilogram). After an oral dose of PQ (or PN1) to mice, the parent form predominated in the blood circulation, and PN1 (or PQ) was detected as a major metabolite. Other factors probably associated with delayed elimination of PQ (intestinal metabolism and enterohepatic circulation) did not play a key role in PQ elimination. These data suggested that the metabolic interconversion of PQ and its *N*-oxide metabolite contributes to but may not significantly prolong its duration in humans.

SIGNIFICANCE STATEMENT

This paper investigated the interconversion metabolism of piperaquine (PQ) and its *N*-oxide metabolite in vitro as well as in mice. The metabolic profiles of PQ were reestablished by this futile cycling, which contributes to but may not significantly prolong its elimination in humans. Enzyme phenotyping indicated a low possibility of interaction of PQ during artemisinin drug-based combination therapy treatment.

Introduction

Artemisinin drug-based combination therapy (ACT) is the first-line treatment of uncomplicated *Plasmodium falciparum* malaria (WHO, 2015). Artemisinin drug plays a key role in the rapid clearance of *P. falciparum*, whereas the partner antimalarial with a prolonged elimination half-life is responsible for the remaining parasites (Gutman et al., 2017; Warsame et al., 2019). The emerging parasite resistance to artemisinin drugs highlights the importance of the partner drugs in ACTs (Hassett and Roepe, 2019; Noisang et al., 2019), such as piperaquine (PQ; Fig. 1) (Mandara et al., 2019; Chebore et al., 2020). PQ has been used as monotherapy for prophylaxis and treatment of malaria until its emerging drug resistance (Pasay et al., 2016). Two ACTs containing PQ are dihydroartemisinin plus PQ (Duo-Cotecxin) and artemisinin plus PQ (Artequick), which are well tolerated and highly effective in the treatment of *P. falciparum* malaria. The in vitro susceptibilities of *P. falciparum* clones *Pf*3D7 (chloroquine sensitive) or *Pf*Dd2 (chloroquine resistant) to PQ were ~10.0 nM (IC_{50}) (Traore et al., 2015; Liu et al., 2018). Plasmodium isolates with IC_{50} values >135.0 nM or 2.3-fold higher than that of *Pf*3D7 were considered to display reduced susceptibility to PQ (Chaorattanakawee et al., 2015).

PQ pharmacokinetics exhibits a large volume of distribution (~700 l/kg), an oral clearance of 29–109 l/h, and an extremely long elimination half-life ($t_{1/2}$, ~30 days) in healthy volunteers and patients with malaria (Tarning et al., 2005; Keating, 2012; Leong et al., 2018). The absolute oral bioavailability of PQ in rats was ~50% (Tarning et al., 2008). Several metabolites have been found for PQ in rats (Tarning et al., 2008; Yang et al., 2016) and humans (Tarning et al., 2006; Liu et al., 2018), which mainly included two *N*-oxidation products [piperaquine *N*-oxide (PN1) and piperaquine *N*,*N*-dioxide (PN2); Fig. 1], a carboxylic acid and two minor hydroxylated products. The pharmacokinetic profiles of PQ and its *N*-oxide metabolites have been reported in rats (Liu et al., 2017) and human subjects (Liu et al., 2018) after oral administrations of PQ.

This work was supported by the National Science Foundation of China [Grant 81773807]. The authors declare no conflicts of interest.
https://doi.org/10.1124/dmd.120.000306.
This article has supplemental material available at dmd.aspetjournals.org.

ABBREVIATIONS: 1-ABT, 1-aminobenzotriazole; ACT, artemisinin drug-based combination therapy; AUC, area under the plasma concentration-time curve; CL_B, biliary clearance; CL_H, hepatic clearance; CL/F, total oral clearance; CL_{int}, intrinsic clearance; $CL_{int,H}$, intrinsic hepatic clearance; $CL_{int,sec}$, intrinsic secretory clearance; CQ, chloroquine; ef_m'', effective coefficient for metabolite formation; FMO, flavin-containing monooxygenase; fu_P, fraction unbound in plasma; HIM, human intestinal microsomes; HLM, human liver microsome; MLM, mouse liver microsome; MMI, methimazole; P450, cytochrome P450; PN1, piperaquine *N*-oxide; PN2, piperaquine *N*,*N*-dioxide; PQ, piperaquine; R_{bp}, blood-to-plasma ratio.

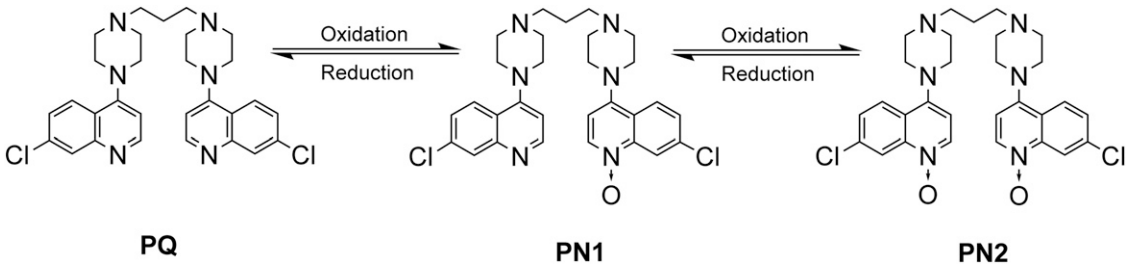

Fig. 1. Interconversion metabolic pathways of PQ and its *N*-oxide metabolites (PN1, PQ *N*-oxide; PN2, PQ *N*,*N*-dioxide).

The parent drug PQ accounted for ~63.8% of the total exposure in healthy humans after four oral doses of dihydroartemisinin (80 mg/dose) plus PQ (640 mg/dose), with a major circulating metabolite PN1 (36.2% of the total exposure) and trace PN2 (2.0%) (Liu et al., 2018). A plasma PQ concentration of >56.2 nM (30 ng/ml) at day 7 is usually used as the threshold level for adequate PQ exposure (Leang et al., 2015). Compared with PQ, PN1 showed comparable antimalarial efficacy in mice infected with *Plasmodium yoelii* (Liu et al., 2018). The role of PQ metabolites (especially PN1) in determining its clinical efficacy and optimization of its dosing regimens remains to be investigated.

The *N*-oxidation of tertiary amines is a common metabolic pathway, which has been mainly attributed to cytochrome P450 monooxygenases (P450s) and/or flavin-containing monooxygenases (FMOs) (Shiraga et al., 2012; Wang et al., 2016). Interestingly, the *N*-oxide metabolite can be reversibly metabolized back to the parent drug, which may be mediated by hepatic P450s enzymes, cytochrome P450 reductase, or intestinal microflora (Parte and Kupfer, 2005; Kim, 2015; Cashman et al., 2020). A phenotyping study using substrate depletion showed that PQ metabolism was mainly mediated by CYP3A4 (Lee et al., 2012). PQ and its metabolite PN1 were also inhibitors of CYP3A4/5 (Aziz et al., 2018). The catalyzing enzymes responsible for PQ *N*-oxidation remain unknown, and the probable reversible transformation of PQ *N*-oxide metabolites back to PQ has not been evaluated.

The aforementioned data indicate that metabolic interconversion probably existed between PQ and its major *N*-oxide metabolite PN1, which may contribute to the extremely slow elimination of PQ in vivo. In the present work, phenotyping with liver microsomes and recombinant enzymes (P450s and FMOs) was performed to investigate the enzymes involved in the interconversion metabolism. The enzyme kinetics for this futile cycling were evaluated in liver microsomes. The physiologic and pharmacokinetic characteristics of PQ and its *N*-oxidation metabolites (PN1 and PN2) were also evaluated, which included plasma protein binding, blood-to-plasma partitioning, and biliary clearance. Based on the data obtained above, quantitative prediction of hepatic clearance of PQ in both mice and humans was performed to evaluate the contribution of futile cycling to the slow elimination of PQ. The pharmacokinetic profiles of PQ and its *N*-oxide metabolite PN1, either as parent form or as metabolite, were investigated in mice after an oral dose of PQ or PN1. Other factors that may contribute to the slow elimination of PQ, i.e., interconversion metabolism in intestinal microsomes, reduction by gut microbiota, and the enterohepatic circulation were also investigated.

Materials and Methods

Chemicals and Reagents. Piperaquine phosphate and chloroquine (CQ) were purchased from the National Institutes for Food and Drug Control (purity >99.0%, Beijing, China). Two metabolites of PQ (PN1 and PN2) were synthesized and purified in our laboratory (purity >99.0%), and their structures were confirmed by high-resolution mass spectrometry and NMR. To ensure that two *N*-oxides were free from the parent compound (<0.1%), both PQ *N*-oxides were repurified by silica gel columns. Liver S9 fractions, cytosol, and pooled intestinal microsomes derived from humans and mice were purchased from XenoTech (Lenexa, KS). Pooled liver microsomes derived from human (HLMs), mice (MLMs), rat, dog, minipig, and monkey were purchased from RILD Research Institute for Liver Diseases (Shanghai, China). Recombinant P450 isoforms (CYP1A2, 2B6, 2C8, 2C9, 2C19, 2D6, and CYP3A4) and cytochrome P450 reductase were purchased from Cypex Ltd. (Dundee, UK). Recombinant FMO isoforms (FMO1, FMO3, and FMO5) were purchased from Corning (Woburn, MA). NADPH, FAD, 1-aminobenzotriazole (1-ABT), methimazole (MMI), ketoconazole, α-naphthoflavone, quinidine, sulfaphenazole, ticlopidine, quercetin, raloxifene, isovanillin, dicoumarol, midazolam, 1′-OH-midazolam, diclofenac, omeprazole, dextromethorphan, and benzydamine were purchased from Sigma-Aldrich (St. Louis, MO). Other chemicals used were purchased from Sigma-Aldrich or Fisher Scientific.

In Vitro Metabolism using S9, Cytosol, Liver Microsomes, and Intestinal Microsomes. PQ (1 μM) or PN1 (1 μM) was incubated with liver S9 fractions (1 mg/ml), cytosol (1 mg/ml), liver microsomes (1 mg/ml) or intestinal microsomes (1 mg/ml) in potassium phosphate buffer (0.1 M, pH 7.4) and NADPH (1 mM) at 37°C for 30 minutes. The incubation was initiated by adding NADPH and stopped by adding two volumes of cold acetonitrile. PN2 (1 μM) was incubated in HLMs and MLMs according to the procedures shown above.

To assess the role of putative P450 enzymes in the interconversion metabolism, incubations of PQ or PN1 with HLMs (0.5 mg/ml) were carried out as described above in the presence of selective chemical inhibitors of total P450 enzymes (1 mM 1-ABT; preincubated for 30 minutes), CYP3A4 (1 μM ketoconazole), CYP2C8 (25 μM quercetin), CYP2D6 (10 μM Quinidine), CYP1A2 (5 μM α-naphthoflavone), CYP2B6 (10 μM ticlopidine), CYP2C9 (20 μM sulfaphenazole), and CYP2C19 (10 μM ticlopidine).

To investigate the potential role of FMO, thermal inactivation that selectively diminishes FMO activity without affecting P450 activity was applied by preheating HLMs (0.5 mg/ml) at 45°C for 5 minutes (without NADPH). Aliquots of preheated or control HLMs were then incubated with PQ or PN1. The selective inhibitor of FMO (0.25 mM MMI) was used to determine the role of FMO in metabolism of PQ or PN1.

The effect of hemoglobin (100 nM), FAD (10 μM), cytochrome P450 reductase (100–500 nM) and/or NADPH (1–5 mM) on the reduction metabolism of PN1 was evaluated in HLMs according to the procedure described above. The (non)selective inhibitors of total P450 enzymes (1 mM 1-ABT; preincubated for 30 minutes), FMO enzymes (0.25 mM MMI), aldehyde oxidase (10 μM raloxifene or 20 μM isovanillin), and NADPH quinone reductase (20 μM dicoumarol) were used in human liver cytosol to evaluate their roles in PN1 reduction.

Positive and negative controls for each liver microsome were assayed alongside probe substrates to confirm the activity of microsomal product. All incubations were carried out in triplicate.

In Vitro Metabolism using Recombinant Human P450 and FMO Enzymes. PQ (1 μM) or PN1 (1 μM) was incubated with recombinant P450s (100 pmol/ml) or recombinant FMOs (0.25 mg/ml) in potassium phosphate buffer (0.1 M, pH 7.4) and NADPH (1 mM) at 37°C for 30 minutes. The incubation was initiated by adding either NADPH (for P450s) or the substrate (for FMOs) and stopped by adding two volumes of cold acetonitrile. Positive controls for each P450 or FMO enzyme was assayed alongside probe substrates to confirm

the viability of the recombinant enzymes. All incubations were carried out in triplicate.

To confirm the role of putative P450 enzymes in the reduction metabolism, incubations of PN1 with recombinant enzymes were carried out as described above in the presence of selective chemical inhibitors of CYP3A4 (1 μM ketoconazole), CYP2C8 (25 μM quercetin), CYP2D6 (10 μM Quinidine), or FMO (0.25 mM MMI).

Reduction Metabolism of PN1 by Gut Microbiota. The reduction metabolism of PN1 by gut microbiota was evaluated based on previous studies (Zhou et al., 2015; Lemke et al., 2016). Briefly, intestinal contents collected from three mice were pooled, suspended in saline water (1 g: 4 l), and then homogenized for 10 minutes. After centrifugation (9000 g) at 4°C for 10 minutes, the supernatant was added to the anaerobic culture medium (1:9, *v*/*v*), which was prepared by dissolving brain heart infusion in water (1 g: 20 ml). The obtained intestinal flora cultural solution was used to incubate PN1 (1 μM) at 37°C under anaerobic condition. The reactions were stopped at 0, 0.5, 1, 2, 4, 8, and 12 hours by adding two volumes of cold acetonitrile. The incubations were performed in triplicate.

Determination of Plasma Protein Binding and Blood-to-Plasma Ratio. Plasma protein binding of PQ, PN1, or PN2 at the concentration of 1 μM was determined in pooled plasma collected from human or mice, using equilibrium dialysis described previously (Ryu et al., 2019). The blood-to-plasma concentration ratio (R_{bp}) of PQ was determined by incubating PQ (1 μM) with fresh whole blood collected from human or mice. The blood samples were incubated at 37°C for 1 hour. Then, both blood and plasma samples were taken for analysis. All incubations were performed in triplicate. R_{bp} was calculated by dividing the concentration of PQ in blood by the concentration of PQ in plasma.

Determination of Intrinsic Clearance using In Vitro Half-Life Method. The substrate depletion of PQ and PN1 in liver and intestinal microsomes derived from both human and mice were evaluated. PQ (1 μM) or PN1 (0.2 μM) was incubated with liver or intestinal microsomes (1.0 mg/ml) in potassium phosphate buffer (0.1 M, pH 7.4) at 37°C. The reactions were started by addition of NADPH (1 mM) after a preincubation of 3 minutes at 37°C, and terminated at 0, 15, 30, 45, and 60 minutes by addition of ice-cold acetonitrile containing internal standard (CQ). The incubations were performed in triplicate. The intrinsic clearance (CL_{int}) was determined as follows: CL_{int} = (ln2 × incubation volume)/($t_{1/2}$ × protein amount). $T_{1/2}$ was determined from the elimination rate constant k = ln2/$t_{1/2}$.

Enzyme Kinetics in Liver Microsomes. The enzyme kinetics of PQ, PN1, and PN2 in liver microsomes derived from both human and mice were evaluated. In time and protein linearity experiments, PQ (1 μM), PN1 (0.2 μM for *N*-oxidation, and 100 μM for the reduction metabolism), or PN2 (100 μM) was incubated in triplicate with liver microsomes (0.1–1 mg/ml) at 37°C. The reaction was initiated by addition of 1 mM NADPH and terminated at 15–60 minutes by addition of two volumes of ice-cold acetonitrile containing internal standard (CQ). For kinetic analysis, PQ, PN1, or PN2 was incubated with liver microsomes (0.5 mg/ml) at six or seven concentrations. Reactions were initiated by adding NADPH (1 mM) and terminated after 30 minutes. The formation rates of PN1 or PN2, expressed as picomoles of each metabolite formed per minute per milligram of protein, were calculated and plotted against target compound concentration. The rate of PQ depletion was also determined. The formation rate of PQ (or PN1), as a reduction metabolite of PN1 (or PN2), was evaluated. Nonlinear regression analysis (WinNonLin, Pharsight, NC) was performed using the Michaels-Menten kinetic equation for the determination of K_m and V_{max}.

Pharmacokinetic Study of PQ and PN1 in Mice. Male Kunming mice weighted 25–30 g (6 to 7 weeks) were supplied by the Laboratory Animal Center of Shandong University (Grade II, Certificate No. SYXK2019-0005). The experimental protocol was approved by the University Ethics Committee (SDU-2017D027) and conformed to the "Principles of Laboratory Animal Care" (NIH publication no. 85-23, revised 1985). Laboratory animals were fasted for 12 hours before drug administration and for a further 2 hours after dosing. Water was freely available during experiments.

For evaluation of the pharmacokinetic profiles of PQ and PN1 in mice, PQ or PN1 was suspended (for an oral dose) or dissolved (for an intravenous dose) in water containing 0.03% acetic acid (pH 5). After an oral dose of PQ or PN1 (40 mg/kg) to mice (n = 6 for each time point), 20 μl of blood samples was withdrawn from the jugular vein inserted with a polyethylene catheter before dosing and at 0.5, 1, 2, 3, 4, 6, 8, 12, 24, 36, 48, 60, 72, 84, 96, 120, 144, 168, 240, 336, 504, and 672 hours postdosing. After an intravenous administration of PN1 or PN2 (5 mg/kg) to mice, blood samples (n = 6 for each time point) were taken at 0, 0.017, 0.25, 0.5, 1, 2, 4, 8 12, 24, 36, and 48 hours postdosing. To evaluate the role of enterohepatic circulation, PQ was given orally to freely moving mice with cannulated bile duct (40 mg/kg; n = 6), and bile samples were collected at 0–4, 4–8, 8–12, 12–24, 24–36, and 36–48 hours. To evaluate the biliary clearance of PN1 and PN2 in mice (n = 6), the bile samples were also collected during 0–48 hours after an intravenous dose (5 mg/kg).

The pharmacokinetic parameters were analyzed by a noncompartmental model using the program TOPFIT (version 2.0; Thomae GmbH, Germany). The peak plasma concentration (C_{max}) and time-to-peak concentration were obtained from experimental observations. The area under the plasma concentration-time curve (AUC_{0-t}) was calculated using the linear trapezoidal rule to approximately the last point. The mean residence time was obtained by dividing the area under the first moment-time curve by the AUC_{0-t}. Total oral body clearance (CL/F) was calculated as dose/AUC_{0-t}. The terminal elimination half-life ($t_{1/2}$) was estimated by log-linear regression in the terminal phase using an average of 4–6 observed concentrations.

Sample Processing and Analysis. After termination by adding two volumes of cold acetonitrile containing internal standard, 50 μl of incubates were centrifuged at 7215*g* for 15 minutes. The supernatant was dried under N_2 at room temperature, and then reconstituted with initial mobile phase before analysis. All incubation samples were analyzed by validated liquid chromatography–high resolution mass spectrometry methods, which were carried out on a Thermo Electron LTQ-Orbitrap XL hybrid mass spectrometer (ThermoFinnigan, Bremen, Germany) equipped with an electrospray ionization interface. The chromatographic and mass spectrometric conditions referred to a previous report (Yang et al., 2016). Representative chromatograms for metabolite identification of PQ and its metabolites in microsomal incubates are shown in Supplemental Fig. 1.

Blood, plasma, and bile samples were subjected to a protein precipitation extraction process, and a liquid chromatography–mass spectrometry method was applied for quantification of PQ and its metabolites. The mass spectrometric analyses were performed on an API5500 Q-Trap triple quadrupole mass spectrometer (AB SCIEX, Concord, ON, Canada) equipped with a TurboIonSpray source. The detailed sample preparation, chromatographic, and mass spectrometric conditions referred to previous reports (Liu et al., 2017, 2018), and the analytical methods were fully validated. Representative chromatograms for quantification of PQ and its metabolites in plasma samples are shown in Supplemental Fig. 2.

Prediction of Hepatic Clearance and Intestinal Clearance. The hepatic clearance (CL_H) of PQ was predicted using the well stirred model (eq. 1):

$$CL_H = \frac{Q_H * fu_B * CL_{int,H}}{Q_H + fu_B * CL_{int,H}} \quad (1)$$

Intrinsic hepatic clearance ($CL_{int,H}$) is the intrinsic clearance obtained from liver microsomal incubations. The fraction unbound in blood (fu_B) was determined by multiplying the fraction unbound in plasma (fu_P) by the plasma-to-blood ratio. Intrinsic clearance values in human/mice liver microsomes were scaled to hepatic intrinsic clearances assuming a hepatic blood flow (Q_H) of 1.28/5.4 l/h per kilogram, 40/45 mg of microsomal protein/g liver, and 21.4/55 g liver/kg body weight, based on previous reports (Barter et al., 2007; Sager et al., 2016; Sawada et al., 2020).

In the presence of a primary metabolite PN1 (Mi) and a sequential metabolite PN2 (Mii), in vitro clearance of PQ ($CL_{int,H}$) was determined either by substrate depletion or metabolite formation (eq. 2), derived from both PN1 ($\mathbf{CL^{P\rightarrow Mi}_{int,met,H}}$) and PN2 ($\mathbf{CL^{P\rightarrow Mii}_{int,met,H}}$).

$$CL_H = \frac{Q_H \cdot fu_B\left(CL^{p\rightarrow Mi}_{int,met,H} + CL^{p\rightarrow Mii}_{int,met,H}\right)}{Q_H + fu_B\left(CL^{p\rightarrow Mi}_{int,met,H} + CL^{p\rightarrow Mii}_{int,met,H}\right)} \quad (2)$$

As a major metabolite of PN1, PN2 was only detected in trace amounts in microsomal incubations with PQ. The intrinsic clearance for PQ to form sequential metabolites was assumed to be zero. The eq. 2 was then simplified as eq. 3:

$$CL_H = \frac{Q_H \cdot fu_B\left(CL^{p\rightarrow Mi}_{int,met,H}\right)}{Q_H + fu_B\left(CL^{p\rightarrow Mi}_{int,met,H}\right)} \quad (3)$$

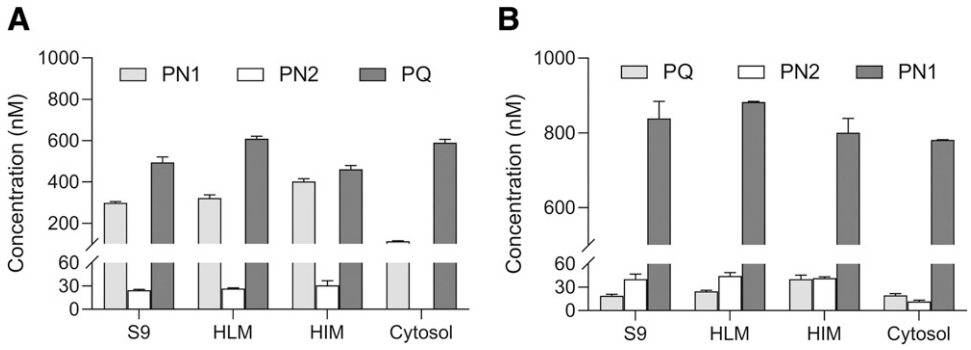

Fig. 2. Interconversion metabolism of PQ and its *N*-oxide metabolite (PN1) in human hepatic S9, HLMs, intestinal microsomes (HIM), and cytosol. (A) metabolite formation of PN1 and PN2 from PQ; (B) metabolite formation of PQ and PN2 from PN1. PQ (1 μM) and PN1 (1 μM) were incubated in liver fractions (1 mg/ml) for 30 minutes. The experiment was performed in triplicate.

The primary metabolite PN1 can interconvert back to the precursor drug PQ ($\mathbf{CL^{Mi\rightarrow P}_{int,met,H}}\{mi\}$), and form a further *N*-oxidation metabolite PN2 with the intrinsic clearance ($\mathbf{CL^{Mi\rightarrow Mii}_{int,met,H}}\{mi\}$). The metabolite PN2 can reduce back to PN1 ($\mathbf{CL^{Mii\rightarrow Mi}_{int,met,H}}\{mii\}$) (Fig. 1). PN1 and PN2 may also be excreted biliarily with $CL_{int,sec,H}\{mi\}$and $CL_{int,sec,H}\{mii\}$, respectively. In the presence of this futile cycling (Supplemental Fig. 3), the effective coefficient for metabolite formation of PN1 (ef_m'') or PN2 (ef_{mi}'') was introduced (eq. 4) based on previous reports (Pang and Durk, 2010; Sun et al., 2010):

$$CL_H = \frac{Q_H \cdot fu_B\left(ef_m'' CL^{P\rightarrow Mi}_{int,met,H}\right)}{Q_H + fu_B\left(ef_m'' CL^{P\rightarrow Mi}_{int,met,H}\right)} \quad (4)$$

The ef_m'' (eq. 5) stands for the fraction that reduces the intrinsic clearance for metabolite formation of PN1 ($\mathbf{CL^{P\rightarrow Mi}_{int,met,H}}$). A low ef_m'' suggests a pronounced effect of futile cycling on PQ disposition.

$$ef_m'' = \frac{CL_{int,sec,H}\{mi\} + CL^{Mi\rightarrow Mii}_{int,met,H}\{mi\}}{CL_{int,sec,H}\{mi\} + CL^{Mi\rightarrow P}_{int,met,H}\{mi\} + CL^{Mi\rightarrow Mii}_{int,met,H}\{mi\}} \quad (5)$$

Similarly, ef_{mi}'' (eq. 6) was used to calculate the effective intrinsic clearance for metabolite formation of PN2 ($\mathbf{CL^{Mi\rightarrow Mii}_{int,met,H}}\{mi\}$).

$$ef_m'' = \frac{CL_{int,sec,H}\{mii\} + CL^{Other}_{int,met,H}\{mii\}}{CL_{int,sec,H}\{mii\} + CL^{Mii\rightarrow Mi}_{int,met,H}\{mii\} + CL^{Other}_{int,met,H}\{mii\}} \quad (6)$$

In this study, only reduction metabolism was found for PN2, and $\mathbf{CL^{Other}_{int,met,H}}\{mii\}$ to form other metabolites was zero. The secretory clearances of PN1 ($CL_{int,sec,H}\{mi\}$) and PN2 ($CL_{int,sec,H}\{mii\}$), i.e., intrinsic biliary clearance ($CL_{int,B}$) in this study, were calculated by in vivo biliary clearance (CL_B) (eq. 7).

$$CL_{B,in\ vivo} = \frac{Q_p \cdot fu_p \cdot CL_{int,B}}{Q_p + fu_p \cdot CL_{int,B}} \quad (7)$$

The CL_B values of PN1 and PN2 in mice were determined by dividing the dose excreted from bile as parent drug by their exposures (AUC_{0-t}) after an intravenous administration. The hepatic plasma flow (Q_P) was calculated by the hepatic blood flow (Q_H) and hematocrit (0.50 for humans, and 0.45 for mice). Due to the invasive techniques to obtain in vivo CL_B, the $CL_{int,sec,H}$ values of PN1 and PN2 in humans were assumed to be similar to that of mice.

The following predictions of hepatic clearance were made: 1) the hepatic clearance of PQ based on substrate depletion, 2) the hepatic clearance of PQ based on metabolite formation without considering the futile cycling, and 3) the hepatic clearance of PQ based on the effective metabolite formation with futile cycling.

In the presence of enterohepatic circulation, the metabolite of PQ (PN1) may be excreted into bile and then reduced back to PQ by gut microbiota. To evaluate the potential role of enterohepatic circulation, the biliary excretion of PQ and its metabolite PN1 was determined in mice after an oral dose of PQ. To predict the worst scenario of futile cycling, excreted PN1 was assumed to reduce back to PQ completely in the intestine. The dose of PQ increased apparently due to its enterohepatic circulation ($Dose_{PN1\rightarrow PQ}$), and the CL/F was calculated by $(Dose + Dose_{PN1\rightarrow PQ})/AUC_{0-t}$.

Results

The *N*-Oxidation Metabolism of PQ and its *N*-Oxide Metabolite (PN1) in S9 Fractions, Cytosol, and Liver/Intestinal Microsomes. PQ and its primary metabolite PN1 were incubated in hepatic S9, cytosol, and microsomal fractions at a concentration of 1 μM to determine the nature of the enzymes mediating the *N*-oxidation. In human S9 or liver/intestinal microsomal fractions, PQ was mainly metabolized to PN1 with trace PN2 in the presence of NADPH (Fig. 2). The incubation with PN1 displayed further *N*-oxidation (PN2). Less *N*-oxidation metabolites were formed in cytosol.

Compared with HLMs, similar metabolic profiles were found for the metabolism of PQ in MLMs, in terms of the formed amount of each metabolite (Supplemental Fig. 4). A higher concentration level of *N*-oxidation metabolites was observed for PQ in liver microsomes derived from minipig and monkey. PN1 was found as a major metabolite for PQ in microsomes derived from rat and dog, without detectable PN2.

N-oxidation metabolism of PQ and its metabolite PN1 by HLMs was also measured in the presence of (non)selective inhibitors, to determine

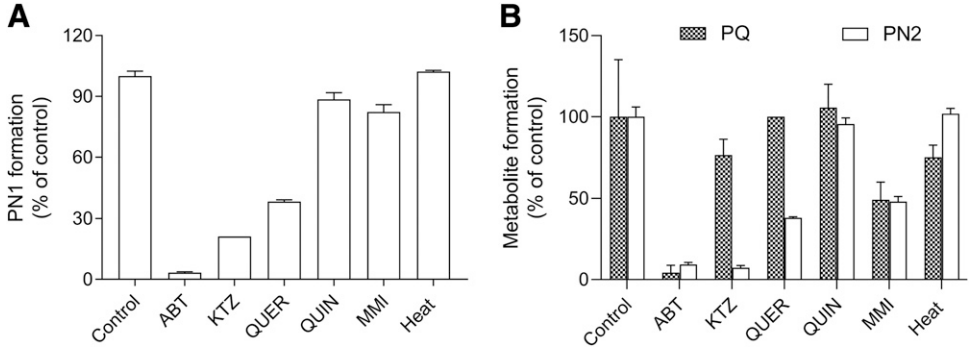

Fig. 3. Metabolite formation of PN1 from PQ, PQ *N*,*N*-dioxide (PN2) from PN1, PQ from PN1 in HLMs, when incubated with (non) selective inhibitors of total P450s (1-ABT), FMOs (MMI), CYP3A4 (ketoconazole, KTZ), CYP2D6 (quinidine, QUIN), CYP2C8 (quercetin, QUER), or pretreated by heat (45°C × 5 minutes). (A) PQ→PN1; (B) PN1→PN2, and PN1→PQ. PQ (1 μM) and PN1 (1 μM) were incubated in HLMs (0.5 mg/ml) for 30 minutes. The experiment was performed in triplicate.

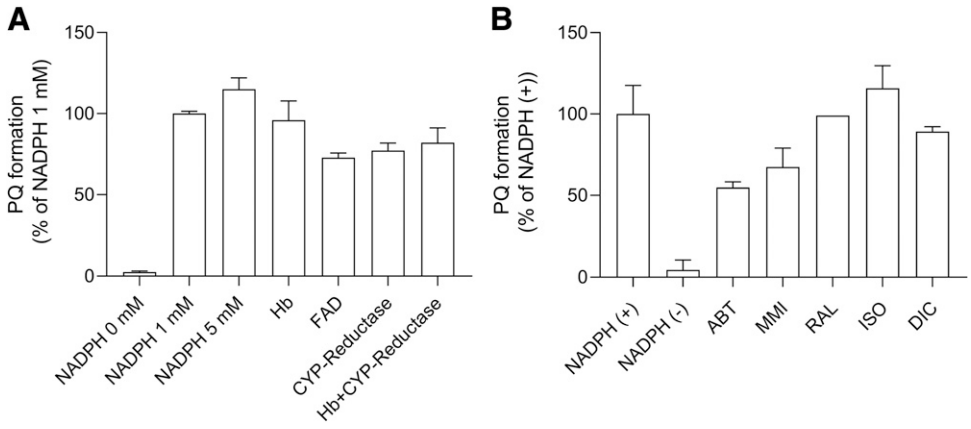

Fig. 4. Metabolite formation of PQ from PN1 in human liver microsomes (A) and human liver cytosol (B), when incubated with cofactors [NADPH, hemoglobin (Hb), FAD, cytochrome P450 reductase] or (non)selective inhibitors of total P450s (1-ABT), FMOs (MMI), aldehyde oxidase (raloxifene, RAL; isovanillin, ISO), NADPH quinone reductase (dicoumarol, DIC). PN1 (100 μM) was incubated in microsomes or cytosol (0.5 mg/ml) for 30 minutes.

the relative contribution of these P450 enzymes toward *N*-oxidation of PQ or PN1. Approximately 96.6%, 78.9%, 61.7%, and 11.5% of *N*-oxidation metabolism of PQ was inhibited by 1-ABT (CYPs), ketoconazole (CYP3A4), quercetin (CYP2C8), and quinidine (CYP2D6), respectively (Fig. 3). The further *N*-oxidation of PN1 was inhibited to a similar extent. Minor inhibition was found for PQ (by 13.8%) or PN1 metabolism (by 51.9%) in the presence of MMI (FMOs). The *N*-oxidation metabolism of PQ and PN1 in HLMs, preheated to 45°C for 5 minutes, was similar to that of control (Fig. 3). The metabolism of the P450 probes by HLMs was not affected by the heat treatment (data not shown).

The Reduction Metabolism in S9 Fractions, Cytosol, and Liver/Intestinal Microsomes. PQ *N*-oxides (PN1 and PN2) were found chemically stable in the buffered saline (pH 7.4). When incubated with PN1 (or PN2) in S9, cytosol, or liver/intestinal microsomes, the reduction metabolite PQ (or PN1) was found. As with the P450s, NADPH was essential for this reaction, and a higher concentration of NADPH (5 mM) increased the formation of PQ to a small extent (Fig. 4). In addition, the reduction metabolism was not induced significantly with the addition of hemoglobin, FAD, or cytochrome P450 reductase (Fig. 4). NADPH alone (buffer) without P450 enzymes did not reduce PN1 to PQ, demonstrating that equivalents alone were not sufficient to start the reduction.

Reduction metabolism of PN1 with HLMs was also evaluated in the presence of (non)selective P450 and FMO inhibitors (Fig. 3). Approximately 95.7% and 50.8% of PQ formation was inhibited by ABT and methimazole, respectively. Selective inhibitors for each P450 enzyme did not show obvious inhibition except for a low inhibition (by 23.6%) by ketoconazole (CYP3A4 inhibitor). The reduction metabolism of PN1 in HLMs, preheated to 45°C for 5 minutes, was reduced to 75.1% of control. Reduction metabolism of PN1 with human cytosol was evaluated in the presence of (non)selective inhibitors of P450s, aldehyde oxidase, and NADPH quinone reductase (Fig. 4). PQ formation was inhibited by 1-ABT (45.2%) and MMI (32.6%), but other selective inhibitors did not show obvious inhibition.

The Metabolism of PQ and PN1 in Recombinant P450 and FMO Enzymes. Of the seven human cDNA-expressed P450 enzymes assessed, CYP3A4 produced PN1 as a major metabolite of PQ (Fig. 5). Correspondingly, the subsequent *N*-oxidation of PN1 to PN2 was also mainly catalyzed by CYP3A4. Lower rates of metabolite formation were found by CYP2D6 (18.5%) and CYP2C8 (1.8%). Other P450 enzymes were inactive (<1.0%). None of the human FMO isoforms (FMO1, FMO3, and FMO5) catalyzed *N*-oxidation metabolism of PQ or PN1 (Fig. 5).

All of the recombinant P450 and FMO enzymes examined catalyzed the reduction of PN1, without noticeably different rates of reaction. The reduction metabolism of PN1 in recombinant CYP3A4, CYP2C8, CYP2D6, and FMO1 was inhibited by ketoconazole (>90.0%), quercetin (>90.0%), quinidine (>70.0%), or methimazole (>80.0%), respectively.

The Reduction Metabolism of PN1 in Gut Microbiota. When PN1 was incubated with gut microbiota, the reduction metabolite PQ was formed at a low rate (14.2 nmol/l per hour). Only 12.1% of PN1 was transformed to PQ after incubation for 8 hours.

Intrinsic Clearance using In Vitro $T_{1/2}$ Method. As an initial investigation into kinetic parameters for PQ and PN1 in both liver microsomes and intestinal microsomes, in vitro $t_{1/2}$ method based on substrate depletion was used. The CL_{int} values in HLMs were calculated

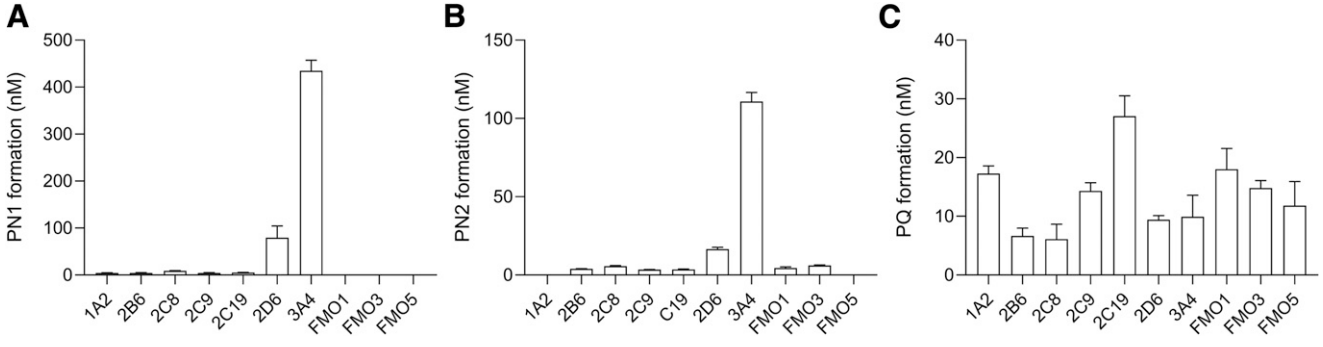

Fig. 5. Interconversion metabolism of PQ and its *N*-oxide metabolite (PN1) in recombinant P450 and FMO isoforms. (A) metabolite formation of PN1 from PQ; (B) metabolite formation of PN2 from PN1; (C) metabolite formation of PQ from PN1. PQ (1 μM) or PN1 (1 μM) was incubated with recombinant P450s (100 pmol/ml) or recombinant FMOs (0.25 mg/ml) for 30 minutes. The experiment was performed in triplicate.

as 14.4 and 4.7 μl/min per milligram protein for PQ and PN1, respectively (Table 1). Comparable intrinsic clearances were found for PQ (10.9 μl/min per milligram protein) and PN1 (5.4 μl/min per milligram protein) in intestinal microsomes. Species difference (human and mice) did not lead to significant changes (<2.0-fold) in the intrinsic clearance (Table 1).

Enzyme Kinetics for *N*-Oxidation Metabolism in Liver Microsomes. The enzyme kinetics for *N*-oxidation metabolism of PQ in HLMs and MLMs were determined by formation of PN1. The subsequent *N*-oxidation metabolism of PN1 was determined by formation of PN2. The formation rate of PN1 or PN2 was linear over the incubation time up to 45 minutes in liver microsomes with the protein concentration of 0.1–1.0 mg/ml. The incubation time of 30 minutes with the protein concentration of 0.5 mg/ml were further used in the enzyme kinetic study, over a concentration range of 0.2–16.0 μM (PQ) and 0.02–2.0 μM (PN1).

The kinetic profiles of PQ and PN1 in liver microsomes (HLMs and MLMs) followed Michaelis-Menten kinetics (Figs. 6 and 7). The $CL_{int,H}$ value of 30.8 μl/min per milligram protein was obtained for PQ *N*-oxidation to form PN1 in HLMs. The subsequent *N*-oxidation to form PN2 in HLMs showed a 2-fold higher $CL_{int,H}$ (56.6 μl/min per milligram protein), with a much lower K_m value (0.1 μM). Compared with human, similar $CL_{int,H}$ was determined for PQ *N*-oxidation in MLMs (29.2 μl/min per milligram protein), and a lower $CL_{int,H}$ was found for PN1 *N*-oxidation (12.6 μl/min per milligram protein). To evaluate the role of *N*-oxidation in PQ metabolism in HLMs, the enzyme kinetics was also performed by PQ depletion, which showed a slightly higher clearance (37.1 vs. 30.8 μl/min per milligram protein).

Enzyme Kinetics for Reduction Metabolism of PN1 in Liver Microsomes. The rate of reduction metabolism in liver microsomes, either from PN1 to PQ or from PN2 to PN1, was linear over the incubation time (5–45 minutes) in liver microsomes with the protein concentration of 0.05–1.0 mg/ml (Supplemental Fig. 5). The rate of this reduction metabolism as a function of PN1 concentrations (1–200 μM) followed Michaelis-Menten kinetics (Figs. 6 and 7). K_m values of 129.9 μM and V_{max} values of 219.1 pmol/min per milligram protein were obtained for PN1 reduction back to PQ in HLMs, leading to the $CL_{int,H}$ value of 1.7 μl/min per milligram protein. Similar $CL_{int,H}$ was obtained for the reduction metabolism of PN1 in MLMs (1.8 μl/min per milligram protein), with a lower K_m value (63.0 μM). Compared with PN1, PN2 showed a similar $CL_{int,H}$ for the reduction metabolism in HLMs (2.1 μl/min per milligram protein), but displayed a higher $CL_{int,H}$ in MLMs (4.7 μl/min per milligram protein).

The Pharmacokinetics of PQ and its Metabolites in Mice. After a single oral dose of PQ to mice, the parent drug PQ and its *N*-oxide metabolite PN1 were the major circulating forms in plasma, and trace PN2 was found. When PN1 was given to mice either orally or intravenously, both reduction metabolism and *N*-oxidation were observed, leading to a major metabolite PQ with quantifiable amount of PN2. The pharmacokinetic profiles of PQ and PN1, either as parent form or as metabolite, in mice after a single dose of PQ or PN1 are shown in Fig. 8 and Supplemental Fig. 6, and the pharmacokinetic parameters are given in Table 2.

The pharmacokinetic profiles of PQ in mice after an oral dose showed multiple concentration peaks of PQ during the absorption phase, with a CL/F of 1.7 l/h per kilogram and a long terminal $t_{1/2}$ (~6.0 days). PN1 was detected quickly after PQ administration (before 0.5 hour), with a metabolic ratio of 0.094, calculated by AUC_{PN1}/AUC_{PQ}. The biotransformation of PQ to PN2 was much lower, and PN2 was detected in only limited numbers of plasma samples at a low concentration level (<10.0 nM). The maximum concentrations of PQ and its metabolite PN1 were reached at 2 hours after oral administration. When PQ was orally administered to mice, only a trace amount (<0.2%) of PQ, PN1, and PN2 was excreted from bile (Supplemental Fig. 7).

An oral administration of PN1 to mice displayed a faster disposition (CL/F, 2.7 l/h per kilogram) than PQ. The metabolic ratios of PQ and PN2, calculated by AUC_{PQ}/AUC_{PN1} and AUC_{PN2}/AUC_{PN1}, were 0.20 and 0.02, respectively. After 96 hours, plasma PQ levels were slightly higher than PN1 plasma concentrations. The absolute oral bioavailability of PN1 was calculated to be 61.3% in mice (Table 2). After an intravenous administration of PN1 or PN2 to mice, a trace amount of PN1 (1.5% of dose) was excreted from bile, and a higher biliary excretion was recovered for PN2 (10.3% of dose) (Supplemental Fig. 7). The biliary clearance of PN1 and PN2 in mice was 0.03 and 0.21 l/h per kilogram, respectively.

The Quantitative Prediction of Hepatic and Intestinal Clearance. In vitro data of PQ derived from both *N*-oxidation and reduction reaction were used to predict the net hepatic clearance of PQ (Supplemental Table 1). The ef_m'' for *N*-oxidation of PQ to form PN1 in HLMs was calculated to be 0.97, with an ef_{mi}'' value of 0.94 for the further *N*-oxidation to form PN2. A lower ef_m'' value was found for formation of PN2 (0.71) and PN1 (0.87) in MLMs.

PQ and its metabolite PN1 were highly protein bound with an fu_P lower than 0.06 in both humans and mice (Table 3). The metabolite PN2 showed a higher fu_P value around 0.2. The R_{bp} of PQ was 0.55 and 4.01 in humans and mice, respectively. The $CL_{int,sec}$ of PN1 and PN2 in mice was calculated to be 0.44 and 1.73, respectively, when normalized for plasma protein binding. In the presence of futile cycling, the unbound hepatic clearance of PQ was predicted to decrease by 2.5% and 12.8% in humans (0.069 l/h per kilogram) and mice (0.024 l/h per kilogram), respectively.

TABLE 1

Intrinsic clearance (microlitre per minute per milligram protein) of PQ and its *N*-oxide metabolite (PN1) in human and mouse microsomes, calculated by substrate depletion

Substrate	HLMs	HIMs	MLMs	MIMs
PQ	14.4 ± 0.6	10.9 ± 0.6	15.3 ± 0.4	17.6 ± 0.6
PN1	4.7 ± 0.9	5.4 ± 0.6	3.3 ± 0.2	3.2 ± 0.8

HIM, human intestinal microsome; MIM, mouse intestinal microsome. The CL_{int} was determined by the elimination half-life of substrate [CL_{int} = (ln2 × incubation volume)/($t_{1/2}$ × protein amount)]. $T_{1/2}$ was determined from the elimination rate constant k = $ln2/t_{1/2}$. The experiment was performed in triplicate.

Discussion

In the present study, PQ and its major *N*-oxide metabolite (PN1) were found to be metabolically interconverted in a cyclic manner. The incubation of PQ and PN1 in liver fractions showed that the *N*-oxidation metabolism mainly happened in microsomes, suggesting the involvement of either P450s or FMOs. The inhibition study indicated the *N*-oxidation metabolism of PQ and PN1 was mainly mediated by CYP3A4 with some involvement of CYP2C8 and CYP2D6. Further consistent evidence was obtained in recombinant human P450 enzymes. Heat treatment had a negative influence on PQ *N*-oxidation, indicating that FMOs were not involved in this metabolic pathway. Findings were also in accord with the incubation in recombinant FMO enzymes. However, preincubation with MMI (a nonselective FMO inhibitor) reduced the formation of *N*-oxides by 13.8% (PN1) or 51.9% (PN2). This may be the confounding effect of MMI on CYP3A4, which was supported by the decreased metabolic activity toward the probe substrates after MMI pretreatment (data not shown).

In the presence of microsomes and NADPH, PN1, or PN2 was rapidly retroreduced to PQ or PN1, respectively. The metabolite formation was

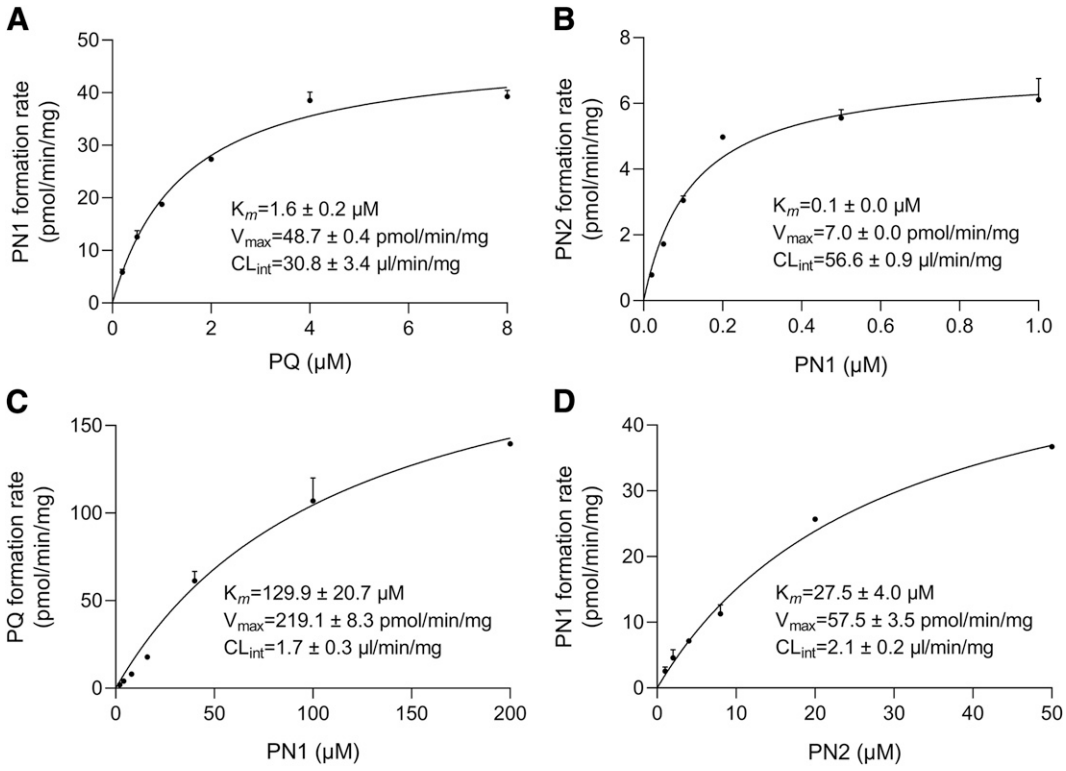

Fig. 6. Enzyme kinetics for metabolite formation of PN1 from PQ, PQ *N,N*-dioxide (PN2) from PN1, PQ from PN1, and PN1 from PN2 in HLMs. (A) PQ→PN1; (B) PN1→PN2; (C) PN1→PQ; (D) PN2→PN1. PQ, PN1, or PN2 was incubated in HLMs (0.5 mg/ml) for 30 minutes. The experiment was performed in triplicate.

almost completely inhibited (>95.0%) after 1-ABT preincubation, and moderate inhibition (~50.0%) was observed by MMI pretreatment, which suggested that the reduction was mainly mediated by P450 with a small involvement of FMOs. The reduction metabolism of PN1 in human cytosol was not affected by raloxifene, isovanillin, or dicoumarol, suggesting no involvement of aldehyde oxidase or NADPH

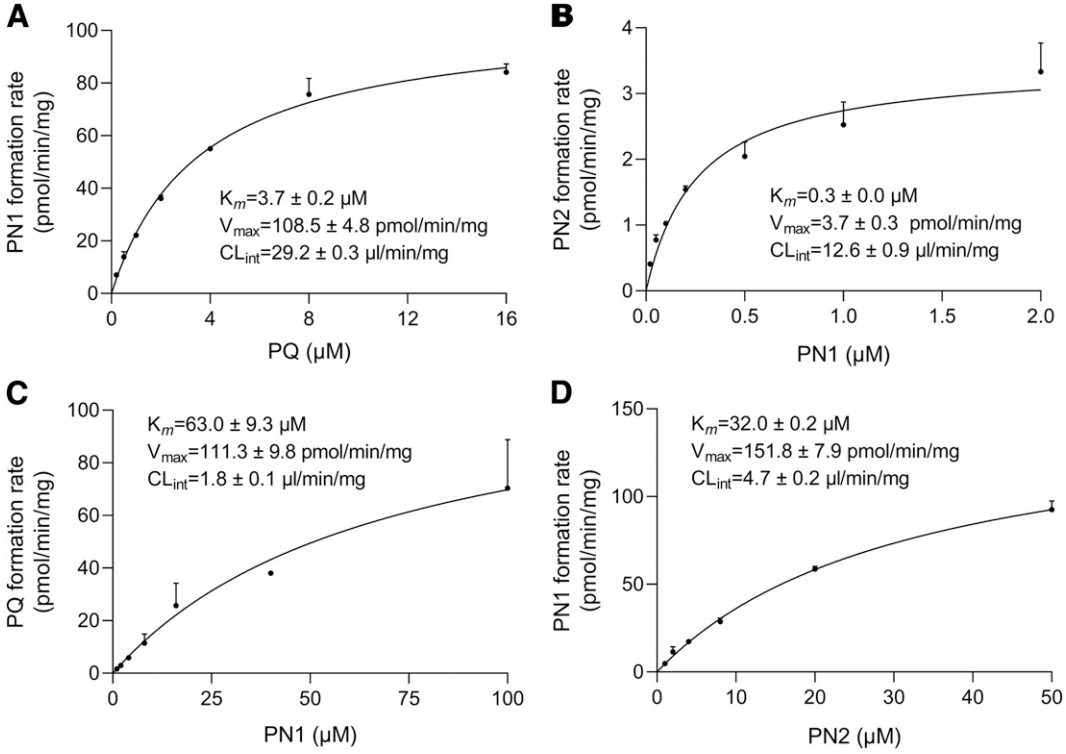

Fig. 7. Enzyme kinetics for metabolite formation of PN1 from PQ, PQ *N,N*-dioxide (PN2) from PN1, PQ from PN1, and PN1 from PN2 in MLMs. (A) PQ→PN1; (B) PN1→PN2; (C) PN1→PQ; (D) PN2→PN1. PQ, PN1, or PN2 was incubated in MLMs (0.5 mg/ml) for 30 minutes. The experiment was performed in triplicate.

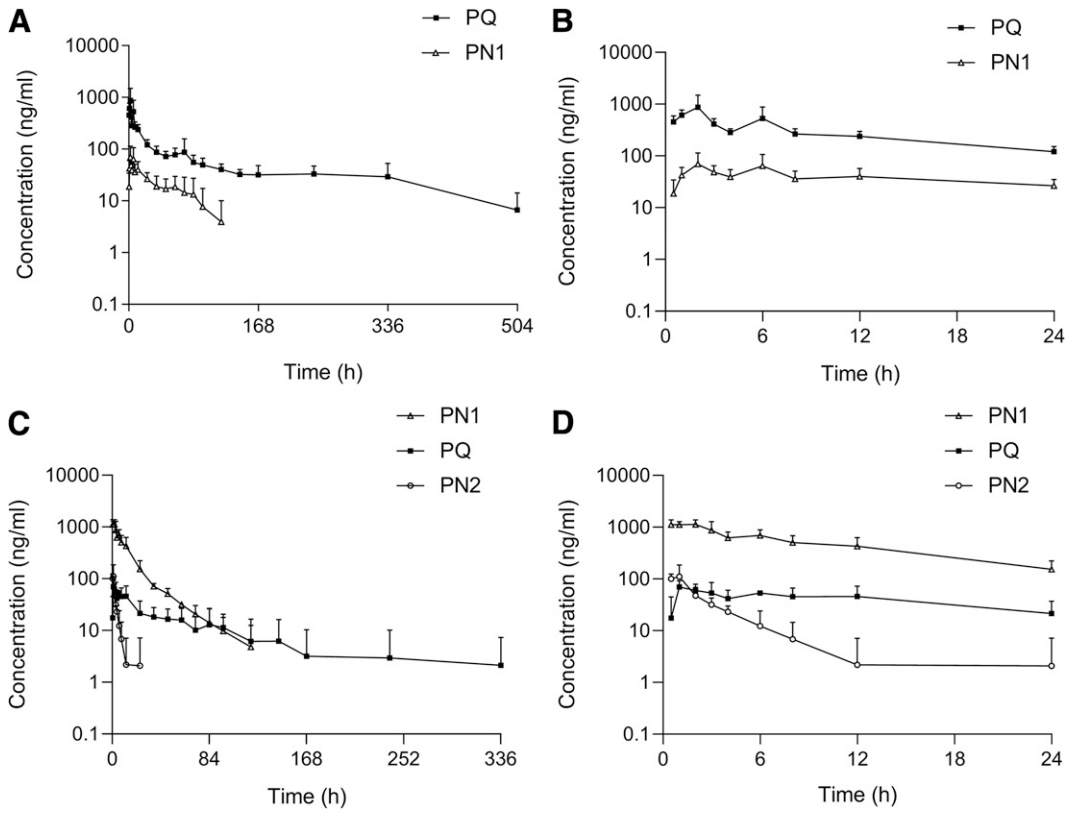

Fig. 8. The pharmacokinetic profiles of PQ and its *N*-oxide metabolites (PN1 and PN2) in mice (n = 6 for each time point) after an oral administration of PQ or PN1 (40 mg/kg). (A) from 0 to 504 hours after an oral dose of PQ; (B) from 0 to 24 hours after an oral dose of PQ; (C) from 0 to 336 hours after an oral dose of PN1; (D) from 0 to 24 hours after an oral dose of PN1.

quinone reductase; however, the reaction was inhibited by 1-ABT (45.2%) and MMI (32.6%), indicating that PN1 reduction back to PQ in cytosol was mainly mediated by the remaining P450/FMO enzymes. The incubation using recombinant enzymes confirmed that the de-oxidation of PN1 to PQ was mediated by all P450s and FMOs evaluated, without specificity. The cofactors FAD, hemoglobin, and/or reductase did not elicit a dramatic increase in the amount of PQ formed in liver microsomes.

As a major enzyme involved in PQ *N*-oxidation, CYP3A4 is the dominant cytochrome P450 in both liver and small intestine (Fan et al., 2010), and the metabolic extraction by the gut wall is substrate-dependent (Shen et al., 1997). In this study, the in vitro half-life method was firstly used as a screening tool to evaluate the hepatic and intestinal clearance of PQ and its metabolite PN1 in microsomes. The CL_{int} values calculated by PQ or PN1 depletion were similar in human liver microsomes and intestinal microsomes. Compared with the liver, the small intestine has lower weight (0.7 vs. 1.8 kg), blood flow rate (0.25 l/min vs. 1.50 l/min), and total CYP450 enzyme level (Fagerholm, 2007). When scaled to the body weight, in vitro CL_{int} for unbounded PQ or PN1 in human liver microsomes was estimated to be ~30 times higher than that in intestinal microsomes, which demonstrated that the contribution of the intestine to the systemic metabolism of PQ and PN1 was negligible in comparison with that by the liver. However, there were several limitations associated with the present in vitro $t_{1/2}$ method. The substrate was set at around K_m to reliably evaluate substrate depletion without either increased variability in determination or exceeding 20% substrate depletion. Moreover, the use of intestinal microsome data may lead to underprediction potential of metabolic capacity, and

TABLE 2

The pharmacokinetic parameters of PQ and its *N*-oxide metabolites (PN1 and PN2) in mice (n = 6 for each sampling point) after an oral (40 mg/kg) or intravenous dose (5 mg/kg) of PQ, PN1, or PN2

Parameters	PQ (oral)		PN1 (oral)			PN1 (intravenous)		PN2 (intravenous)	
	PQ	PN1	PN1	PQ	PN2	PN1	PQ	PN2	PN1
AUC_{0-t} (μg/ml·h)	23.50	2.20	15.01	2.99	0.32	3.06	0.17	1.26	0.52
C_{max} (ng/ml)	866.9	69.5	1132.0	69.7	110.1	N.A.	25.0	N.A.	55.6
T_{max} (h)	2.0	2.0	2.0	1.0	1.0	N.A.	N.A.	N.A.	N.A.
MRT (h)	134.0	N.A.	17.0	N.A.	N.A.	21.2	10.5	1.0	8.7
CL/F_{oral} or $CL_{intravenous}$ (l/h per kilogram)	1.7	N.A.	2.7	N.A.	N.A.	1.6	N.A.	4.1	N.A.
$t_{1/2}$ (h)	144.2	N.A.	22.9	N.A.	N.A.	18.9	N.A.	3.4	N.A.
V_d (l/kg)	N.A.	N.A.	N.A.	N.A.	N.A.	34.8	N.A.	4.1	N.A.

MRT, mean residence time; N.A., not acquired; T_{max}, time to maximum plasma concentration; V_d, volume of distribution.

TABLE 3

Plasma protein binding of PQ and its *N*-oxide metabolites (PN1 and PN2) in humans and mice

Plasma protein binding of PQ, PN1, or PN2 at the concentration of 1 μM was determined in pooled plasma collected from human or mice, using equilibrium dialysis. The experiment was performed in triplicate.

Species	PQ	PN1	PN2
Human	97.38% ± 0.85%	96.76% ± 0.10%	84.19% ± 1.37%
Mice	97.46% ± 1.29%	94.55% ± 0.65%	76.56% ± 1.25%

the well stirred model may not be applicable for prediction of gut-wall metabolism (Fagerholm, 2007).

To evaluate intrinsic hepatic clearance of PQ in the presence of interconversion metabolism, the Michaelis-Menten regression analyses using metabolite formation were performed. The K_m value (1.3 μM) derived from PQ depletion in HLMs was similar to that obtained by PN1 formation (1.6 μM), yielding a similar $CL_{int,H}$ value. The *N*-oxidation pathway predominated in PQ metabolism, and the unaccounted presence of additional metabolites (such as carboxylation) did not play an important role in PQ metabolism. Compared with *N*-oxidation of PQ to form PN1 in HLMs (K_m, 1.6 μM), the sequential *N*-oxidation of PN1 to form PN2 showed a ~2-fold higher $CL_{int,H}$ but with a much lower K_m value (0.1 μM). Saturable drug metabolism would mostly likely occur during the first-pass extraction of PQ (C_{max}, ~1.0 μM) and PN1 (C_{max}, ~0.2 μM) in humans, leading to a transit reduction in the apparent intrinsic clearance. PQ clearance has been found dose-dependent, and it was significantly lower after a higher oral dose of PQ (Nguyen et al., 2008). Compared with *N*-oxidation of PQ to form PN1, the reduction metabolism of PN1 back to PQ displayed a much lower $CL_{int,H}$ (1.7 vs. 30.8 μl/min per milligram protein). A similar $CL_{int,H}$ was obtained for PN2 reduction back to PN1 (2.1 μl/min per milligram protein). The K_m values for reduction metabolism (129.9 μM for PN1, and 27.5 μM for PN2) were ~400-fold higher than the C_{max} of each substrate. Enzyme saturation for reduction metabolism of PN1 or PN2 was not anticipated.

The solution for hepatic clearance based on a simple liver model in presence of futile cycling has been introduced (Pang and Durk, 2010), and a coefficient ef_m'' that reduces the intrinsic clearances for metabolite formation was involved. Taking all data obtained from in vitro physiologic and enzyme kinetic studies, the contribution of futile cycling to the hepatic drug clearance of PQ was estimated. A minor decrease in unbound CL_H (by 12.8%) was found for PQ in mice; however, a negligibly decreased elimination of PQ was predicted in humans (by 2.5%). Biliary clearance of PQ metabolites in humans was not available, and the intrinsic biliary clearance values obtained from mice were used for the prediction. With loss of biliary secretory function, the net hepatic clearance of PQ was expected to decrease due to increased contribution of futile cycling. Other confounders included nonspecific binding, inappropriate kinetic modeling, and failure to account for transporters and extrahepatic metabolism.

To fully explain the slow elimination of PQ, it is necessary to understand the pharmacokinetic characteristics of both PQ and PN1 in vivo. After four recommended oral doses of PQ to healthy subjects, PN1 was a major circulating metabolite, accounting for ~36.2% of total exposure (Liu et al., 2018). However, no study has been performed to examine the pharmacokinetics of PN1. Data derived from the present in vitro study suggested that mouse could be a suitable animal model, and it was used for the further pharmacokinetic study of PQ and PN1. The parent form predominated in the blood circulation (~85.0% of total exposure). PN1 was observed as a major metabolite for PQ (8.6% of total exposure), and PQ was present as a reduction metabolite for PN1 (16.3% of total exposure). The disposition of PN1 differed from PQ with a higher CL/F and a shorter elimination half-life; hence, the back conversion of PN1 to PQ could inevitably prolong the elimination of PQ. Nevertheless, caution should be taken when extrapolating data from mice to humans due to species differences in functions, expression, and tissue distribution of individual P450 isoforms (Martignoni et al., 2006). Moreover, administration of PN1 (preformed metabolite) may or may not directly reflect the metabolite kinetics of PQ, due to the heterogeneity of enzymes, the presence of membrane barriers and transporter-mediated uptake (Pang et al., 2008).

PQ exhibited multiple peaks in its plasma concentration-time profiles, which may be attributed to irregular gastric emptying, changes in gastrointestinal pH, and/or the presence of enterohepatic recycling due to the retroconversion metabolism. PN1 could be reduced back to PQ by gut microbiota at a slow rate. With <0.2% of total dose excreted from bile, any enterohepatic circulation would not contribute significantly to prolongation of the terminal half-life. The extensive tissue binding of PQ should play a key role in its extremely slow elimination, which was in accordance with previous studies (Karunajeewa et al., 2008).

Based on our in vitro findings and the results in mice, it can be speculated that the retroconversion metabolism of PQ and its pharmacologically active metabolite PN1 in humans would be a probable occurrence. Individuals who have a high intrinsic capacity for CYP3A4 may clear PQ and PN1 readily and fail to achieve therapeutic plasma concentrations. Fortunately, artemisinin drugs used in the fixed ACT regimens were neither a good substrate of CYP3A4 nor an inhibitor of CYP3A4 (Xing et al., 2012), indicating a low possibility of interaction of PQ in ACTs. Compared with mice, PN1 existed in humans as a disproportionate metabolite (36.2% vs. 8.6% of total exposure). The significance of the interconversion metabolism in monitoring plasma levels of PQ and clinical outcome needs to be further evaluated.

In summary, this is the first report on the retroconversion metabolism of PQ and its pharmacologically active metabolite PN1. The sequential *N*-oxidation metabolism of PQ was mainly attributed to CYP3A4. The reduction metabolism of PN1 back to PQ was mediated by P450s/FMOs. The rate of *N*-oxidation was ~20 times faster than that of the reduction metabolism in HLMs. Quantitative prediction of hepatic clearance of PQ indicated its slightly decreased elimination in the presence of futile cycling. The intestinal metabolism and enterohepatic circulation should not contribute significantly to the slow elimination of PQ.

Authorship Contributions

Participated in research design: Xing.
Conducted experiments: Xie, Zhang, Liu.
Performed data analysis: Xie, Zhang, Xing.
Wrote or contributed to the writing of the manuscript: Xie, Zhang, Xing.

References

Aziz MY, Hoffmann KJ, and Ashton M (2018) Inhibition of CYP3A by antimalarial piperaquine and its metabolites in human liver microsomes with IVIV extrapolation. *J Pharm Sci* **107**: 1461–1467.

Barter ZE, Bayliss MK, Beaune PH, Boobis AR, Carlile DJ, Edwards RJ, Houston JB, Lake BG, Lipscomb JC, Pelkonen OR, et al. (2007) Scaling factors for the extrapolation of in vivo metabolic drug clearance from in vitro data: reaching a consensus on values of human microsomal protein and hepatocellularity per gram of liver. *Curr Drug Metab* **8**:33–45.

Cashman JR, Gohdes M, de Kater A, and Schoenhard G (2020) N-oxygenation of oxycodone and retro-reduction of oxycodone N-oxide. *Drug Metab Dispos* **48**:106–115.

Chaorattanakawee S, Saunders DL, Sea D, Chanarat N, Yingyuen K, Sundrakes S, Saingam P, Buathong N, Sriwichai S, Chann S, et al. (2015) Ex vivo drug susceptibility testing and molecular profiling of clinical Plasmodium falciparum isolates from Cambodia from 2008 to 2013 suggest emerging piperaquine resistance. *Antimicrob Agents Chemother* **59**: 4631–4643.

Chebore W, Zhou Z, Westercamp N, Otieno K, Shi YP, Sergent SB, Rondini KA, Svigel SS, Guyah B, Udhayakumar V, et al. (2020) Assessment of molecular markers of anti-malarial drug resistance among children participating in a therapeutic efficacy study in western Kenya. *Malar J* **19**:291.

Fagerholm U (2007) Prediction of human pharmacokinetics--gut-wall metabolism. *J Pharm Pharmacol* **59**:1335–1343.

Fan J, Chen S, Chow ECY, and Pang KS (2010) PBPK modeling of intestinal and liver enzymes and transporters in drug absorption and sequential metabolism. *Curr Drug Metab* **11**:743–761.
Gutman J, Kovacs S, Dorsey G, Stergachis A, and Ter Kuile FO (2017) Safety, tolerability, and efficacy of repeated doses of dihydroartemisinin-piperaquine for prevention and treatment of malaria: a systematic review and meta-analysis. *Lancet Infect Dis* **17**:184–193.
Hassett MR and Roepe PD (2019) Origin and spread of evolving artemisinin-resistant Plasmodium falciparum malarial parasites in Southeast Asia. *Am J Trop Med Hyg* **101**:1204–1211.
Karunajeewa HA, Ilett KF, Mueller I, Siba P, Law I, Page-Sharp M, Lin E, Lammey J, Batty KT, and Davis TM (2008) Pharmacokinetics and efficacy of piperaquine and chloroquine in Melanesian children with uncomplicated malaria. *Antimicrob Agents Chemother* **52**:237–243.
Keating GM (2012) Dihydroartemisinin/Piperaquine: a review of its use in the treatment of uncomplicated Plasmodium falciparum malaria. *Drugs* **72**:937–961.
Kim DH (2015) Gut microbiota-mediated drug-antibiotic interactions. *Drug Metab Dispos* **43**: 1581–1589.
Leang R, Taylor WRJ, Bouth DM, Song L, Tarning J, Char MC, Kim S, Witkowski B, Duru V, Domergue A, et al. (2015) Evidence of Plasmodium falciparum malaria multidrug resistance to artemisinin and piperaquine in Western Cambodia: dihydroartemisinin-piperaquine open-label multicenter clinical assessment. *Antimicrob Agents Chemother* **59**:4719–4726.
Lee TM, Huang L, Johnson MK, Lizak P, Kroetz D, Aweeka F, and Parikh S (2012) In vitro metabolism of piperaquine is primarily mediated by CYP3A4. *Xenobiotica* **42**:1088–1095.
Lemke A, Burkhardt B, Bunzel D, Pfeiffer E, Metzler M, Huch M, Kulling SE, and Franz CAMP (2016) Alternaria toxins of the alternariol type are not metabolised by human faecal microbiota. *World Mycotoxin J* **9**:41–49.
Leong FJ, Jain JP, Feng Y, Goswami B, and Stein DS (2018) A phase 1 evaluation of the pharmacokinetic/pharmacodynamic interaction of the anti-malarial agents KAF156 and piperaquine. *Malar J* **17**:7.
Liu H, Zang M, Yang A, Ji J, and Xing J (2017) Simultaneous determination of piperaquine and its N-oxidated metabolite in rat plasma using LC-MS/MS. *Biomed Chromatogr* **31**:e3974.
Liu H, Zhou H, Cai T, Yang A, Zang M, and Xing J (2018) Metabolism of piperaquine to its antiplasmodial metabolites and their pharmacokinetic profiles in healthy volunteers. *Antimicrob Agents Chemother* **62**:e00260–e00318.
Mandara CI, Francis F, Chiduo MG, Ngasala B, Mandike R, Mkude S, Chacky F, Molteni F, Njau R, Mohamed A, et al. (2019) High cure rates and tolerability of artesunate-amodiaquine and dihydroartemisinin-piperaquine for the treatment of uncomplicated falciparum malaria in Kibaha and Kigoma, Tanzania. *Malar J* **18**:99.
Martignoni M, Groothuis GMM, and de Kanter R (2006) Species differences between mouse, rat, dog, monkey and human CYP-mediated drug metabolism, inhibition and induction. *Expert Opin Drug Metab Toxicol* **2**:875–894.
Nguyen TC, Nguyen NQ, Nguyen XT, Bui D, Travers T, and Edstein MD (2008) Pharmacokinetics of the antimalarial drug piperaquine in healthy Vietnamese subjects. *Am J Trop Med Hyg* **79**:620–623.
Noisang C, Prosser C, Meyer W, Chemoh W, Ellis J, Sawangjaroen N, and Lee R (2019) Molecular detection of drug resistant malaria in Southern Thailand. *Malar J* **18**:275.
Pang KS and Durk MR (2010) Physiologically-based pharmacokinetic modeling for absorption, transport, metabolism and excretion. *J Pharmacokinet Pharmacodyn* **37**:591–615.
Pang KS, Morris ME, and Sun H (2008) Formed and preformed metabolites: facts and comparisons. *J Pharm Pharmacol* **60**:1247–1275.
Parte P and Kupfer D (2005) Oxidation of tamoxifen by human flavin-containing monooxygenase (FMO) 1 and FMO3 to tamoxifen-N-oxide and its novel reduction back to tamoxifen by human cytochromes P450 and hemoglobin. *Drug Metab Dispos* **33**:1446–1452.
Pasay CJ, Rockett R, Sekuloski S, Griffin P, Marquart L, Peatey C, Wang CYT, O'Rourke P, Elliott S, Baker M, et al. (2016) Piperaquine monotherapy of drug-susceptible Plasmodium falciparum infection results in rapid clearance of parasitemia but is followed by the appearance of gametocytemia. *J Infect Dis* **214**:105–113.
Ryu S, Riccardi K, Patel R, Zueva L, Burchett W, and Di L (2019) Applying two orthogonal methods to assess accuracy of plasma protein binding measurements for highly bound compounds. *J Pharm Sci* **108**:3745–3749.
Sager JE, Price LSL, and Isoherranen N (2016) Stereoselective metabolism of bupropion to OH-bupropion, threohydrobupropion, erythrohydrobupropion, and 4′-OH-bupropion in vitro. *Drug Metab Dispos* **44**:1709–1719.
Sawada T, Yamaura Y, Higuchi S, Imawaka H, and Yamazaki H (2020) Predicting successful/unsuccessful extrapolation for in vivo total clearance of model compounds with a variety of hepatic intrinsic metabolism and protein bindings in humans from pharmacokinetic data using chimeric mice with humanised liver. *Xenobiotica* **50**:526–535.
Shen DD, Kunze KL, and Thummel KE (1997) Enzyme-catalyzed processes of first-pass hepatic and intestinal drug extraction. *Adv Drug Deliv Rev* **27**:99–127.
Shiraga T, Yajima K, Teragaki T, Suzuki K, Hashimoto T, Iwatsubo T, Miyashita A, and Usui T (2012) Identification of enzymes responsible for the N-oxidation of darexaban glucuronide, the pharmacologically active metabolite of darexaban, and the glucuronidation of darexaban N-oxides in human liver microsomes. *Biol Pharm Bull* **35**:413–421.
Sun H, Zeng YY, and Pang KS (2010) Interplay of phase II enzymes and transporters in futile cycling: influence of multidrug resistance-associated protein 2-mediated excretion of estradiol 17β-D-glucuronide and its 3-sulfate metabolite on net sulfation in perfused TR(-) and Wistar rat liver preparations. *Drug Metab Dispos* **38**:769–780.
Tarning J, Bergqvist Y, Day NP, Bergquist J, Arvidsson B, White NJ, Ashton M, and Lindegårdh N (2006) Characterization of human urinary metabolites of the antimalarial piperaquine. *Drug Metab Dispos* **34**:2011–2019.
Tarning J, Lindegårdh N, Annerberg A, Singtoroj T, Day NPJ, Ashton M, and White NJ (2005) Pitfalls in estimating piperaquine elimination. *Antimicrob Agents Chemother* **49**:5127–5128.
Tarning J, Lindegårdh N, Sandberg S, Day NJ, White NJ, and Ashton M (2008) Pharmacokinetics and metabolism of the antimalarial piperaquine after intravenous and oral single doses to the rat. *J Pharm Sci* **97**:3400–3410.
Traore K, Lavoignat A, Bonnot G, Sow F, Bess GC, Chavant M, Gay F, Doumbo O, and Picot S (2015) Drying anti-malarial drugs in vitro tests to outsource SYBR green assays. *Malar J* **14**:90.
Wang P, Zhao Y, Zhu Y, Sun J, Yerke A, Sang S, and Yu Z (2016) Metabolism of dictamnine in liver microsomes from mouse, rat, dog, monkey, and human. *J Pharm Biomed Anal* **119**: 166–174.
Warsame M, Hassan AM, Hassan AH, Jibril AM, Khim N, Arale AM, Gomey AH, Nur ZS, Osman SM, Mohamed MS, et al. (2019) High therapeutic efficacy of artemether-lumefantrine and dihydroartemisinin-piperaquine for the treatment of uncomplicated falciparum malaria in Somalia. *Malar J* **18**:231.
WHO (2015) *Guidelines for the Treatment of Malaria*, 3rd ed, World Health Organization, Geneva, Switzerland.
Xing J, Kirby BJ, Whittington D, Wan Y, and Goodlett DR (2012) Evaluation of P450 inhibition and induction by artemisinin antimalarials in human liver microsomes and primary human hepatocytes. *Drug Metab Dispos* **40**:1757–1764.
Yang A, Zang M, Liu H, Fan P, and Xing J (2016) Metabolite identification of the antimalarial piperaquine in vivo using liquid chromatography-high-resolution mass spectrometry in combination with multiple data-mining tools in tandem. *Biomed Chromatogr* **30**:1324–1330.
Zhou J, Ma YH, Zhou Z, Chen Y, Wang Y, and Gao X (2015) Intestinal absorption and metabolism of epimedium flavonoids in osteoporosis rats. *Drug Metab Dispos* **43**:1590–1600.

Address correspondence to: Dr. Jie Xing, School of Pharmaceutical Sciences, Shandong University, 44# West Wenhua Rd., Jinan, 250012, P.R. China. E-mail: xingjie@sdu.edu.cn